J Mater Sci (2010) 45:4761–4769
DOI 10.1007/s10853-010-4521-5

ULTRAFINE GRAINED MATERIALS

Strengthening mechanisms and optimization of structure and properties in a nanostructured IF steel

X. Huang · N. Kamikawa · N. Hansen

Received: 15 February 2010 / Accepted: 12 April 2010 / Published online: 27 April 2010

Abstract Nanostructured interstitial free (IF) steel has been produced by accumulative roll-bonding (ARB) for 6 cycles, and post-process treatments by recovery annealing and cold rolling up to 50% thickness reductions have been employed to explore the optimization of structure and mechanical properties. Structural parameters including boundary spacing, misorientation angle, and dislocation density have been quantified by means of transmission electron microscopy and mechanical properties have been determined by tensile testing for the as-ARB processed samples and for the post-process treated samples. Annealing-induced hardening and low-strain cold rolling (<30%) induced softening have been observed, which is accounted for by the availability of mobile dislocations and dislocation sources in different sample conditions. Tailoring the structural scale and dislocation density by additional cold rolling has been verified to be a promising way for optimizing the mechanical properties of nanostructured IF steels produced by warm ARB. Based on the experimental findings, guidelines are discussed for optimizing structure and mechanical properties of samples deformed to very high strains.

X. Huang (✉) · N. Hansen
Risø National Laboratory for Sustainable Energy, Materials Research Division, Danish-Chinese Center for Nanometals, Technical University of Denmark, 4000 Roskilde, Denmark
e-mail: xihu@risoe.dtu.dk; xiaoxu.huang@risoe.dk

N. Kamikawa
Institute for Materials Research, Tohoku University, 2-1-1 Katahira, Aoba-ku, Sendai 980-8577, Japan

Introduction

Nanostructured metals produced by plastic deformation to ultrahigh strains constitute a special class of nanomaterials with special structures and properties. It has been well established that this class of nanostructured metals contain a mixture of high-angle boundaries (often >60%) and low-angle dislocation boundaries [1–7]. Furthermore, the presence of a density of interior dislocations within the volumes between the boundaries is a common structural feature, although the dislocation density varies with the metal, processing technique, and condition [4, 5, 8–12]. These characteristic structural features are distinctly different from those of recrystallized materials, which in general are characterized by a rather small fraction of low-angle boundaries and a very low density of dislocations within the grains. The characteristic properties of deformed nanostructured metals are high-yield strength, which is often several times higher than that of their coarse grained counterparts, and limited uniform elongation (typically less than a few percent), which is often followed by a relatively large post-necking elongation [13–16].

The correlation between structural parameters and mechanical properties, in particular strength has been modeled [1, 7, 17, 18], which suggests that both grain boundary strengthening related to the refined structure and dislocation strengthening related to the low-angle dislocation boundaries and the dislocations between the boundaries must be considered to understand the high strength observed in nanostructured metals. In recent studies [4, 19], the proposed structure–strength relations [17, 18] were applied to calculate the yield stress values and compared with the experimental values for nanostructured commercial purity Al [4] and high-purity Al [19]. This comparison showed that for annealed samples the calculated values are

lower than the experimental values, suggesting a supplementary strengthening mechanism to be added to boundary and dislocation strengthening. Based on detailed structural analysis, a new mechanism, termed dislocation source limited strengthening [19], has been proposed to account for the difference between the calculated and experimental strength values. This strengthening mechanism has alternatively been verified from experimental observations that when dislocations are introduced to an annealed sample a decrease rather than an increase in the yield stress occurs, which is referred to as softening by deformation [4].

In a recent study [20], we demonstrated the effect of a light cold rolling on the structure and mechanical properties of nanostructured interstitial free (IF) steel produced by accumulative roll-bonding (ARB) at a warm temperature of 500 °C. It was found that the as-ARB processed IF steel sheet shows a high-tensile strength but a rapid onset of necking and a low total elongation (2.8%), and that imposing 15% deformation by cold rolling leads to a slight decrease in the strength and a stabilization of the deformation, which leads to an increase in both the uniform and total elongation (6%). Preliminary TEM observations showed that loose dislocations are present in the as-ARB samples and the dislocation density is increased after 15% cold rolling. Relating these structural observations to the change in the strength induced by cold rolling suggests that the dislocation source limited strengthening played a role even in the as-processed ARB state. In this study, we produced a new batch of ARB IF steel sheets under similar conditions to that used in the previous study [20]. The ARB processed sheet samples were subjected to post-process treatments by a recovery anneal at 400 °C, which is then followed by cold rolling at room temperature to different thickness reductions. These treatments were designed to further investigate the strengthening mechanisms on the one hand, and to explore the optimal treatment and structural condition for the improvement of strength and ductility on the other hand. Quantification of structural parameters including the boundary spacing, boundary misorientation angle and distribution, and dislocation density was carried out in order to understand the strengthening mechanisms and to establish the correlation between the structural and mechanical properties.

Processing and characterization

A fully recrystallized ultralow carbon IF steel (Fe–0.002 wt% C–0.003 N–0.01 Si–0.17 Mn–0.012 P–0.01 Cu–0.02 Ni–0.072 Ti) with an average grain size of 20 μm was used as a starting material in the present study. Sheets with a thickness of 1 mm, a width of 30 mm, and a length of ~300 mm were subjected to ARB processing. After being degreased and wire-brushed, two sheets of the starting material were stacked and roll-bonded by applying a large thickness reduction, 50%, in a single pass at 500 °C. A two-high mill with rolls 310 mm in diameter was used for the roll-bonding and the rolling speed was set at 17.5 m min^{-1}, which corresponds to a nominal strain rate of about 19 s^{-1}. The roll-bonding was carried out under dry surface conditions (non-lubricated). The roll-boned sheet was immediately cooled in cold water. The above process steps constitute 1 cycle of ARB processing. To continue the processing, the roll-bonded sheet was cut into half length and provided for the next ARB cycle. In this study, 6 cycles were performed, generating a total thickness reduction of 98.4% or a total equivalent strain of 4.8. The rolling direction (RD) of the sheet was maintained between ARB cycles. To investigate the post-process treatment effect on the evolution of microstructure and mechanical properties, the 6-cycle ARB processed samples were annealed at 400 °C for 0.5 h in an electric furnace, and then cold-rolled to different thickness reductions in the range from 5 to 50%.

The microstructural characterization was carried out by transmission electron microscopy (TEM). The longitudinal section that contained the normal direction (ND) and the RD of the deformed sheets was selected as the observation plane, as it is the best section to reveal the detailed structural features for rolled samples [21]. Thin TEM foils were prepared by electropolishing and examined with a JEOL 2000FX electron microscope operating at 200 kV. An online Kikuchi-line analysis system [22] installed in the microscope was used for crystallographic orientation measurements. The dislocation density in several selected samples was measured using a linear intercept method on TEM images of individual grains taken under multi-beam diffraction conditions to reveal the dislocation content within the grains. The TEM foil thicknesses used for the dislocation density analysis were determined based on convergent beam electron diffraction.

The mechanical properties were characterized by tensile testing. Tensile specimens with a gauge dimension of 10-mm long and 5-mm wide were prepared with the tensile direction parallel to the RD. The samples were tested at room temperature at a constant crosshead speed of 0.5 mm min^{-1}, corresponding to an initial strain rate of 8.3×10^{-4} s^{-1}. Tensile elongation was precisely measured by an extensometer that allowed to a maximum elongation of 10% to be measured and was calibrated before testing. The proof stress at 0.2% engineering strain (hereafter, yield stress, $\sigma_{0.2}$), ultimate tensile strength (UTS), σ_{UTS}), uniform elongation, and total elongation were determined from the experimental data. Two or more samples were tested for each condition, and the average values for strength and elongation are reported.

Results

The results are described in the following three subsections for different sample states. In each case, the structural characterization is presented first and then the mechanical behavior is shown.

As-ARB processed sample

Figure 1 shows an example of TEM analysis of a 6-cycle ARB sample. The overall structure is characterized by a lamellar structure, as shown in Fig. 1a, which is subdivided by two types of boundaries: lamellar boundaries almost parallel to the RD and short transverse boundaries interconnecting the lamellar boundaries. The spacings of lamellar boundaries (d_t) and interconnecting boundaries (d_l) were measured along the RD and the ND, respectively, and the average values were found to be $d_t = 210$ nm and $d_l = 620$ nm, showing an elongated structural morphology with an aspect ratio of approximately 3. The sketch shown in Fig. 1b illustrates the map of boundaries seen in the area marked by a white rectangular frame in Fig. 1a. The misorientation angles across the boundaries were calculated from the orientations of individual crystallites measured based on Kikuchi diffraction [22]. In Fig. 1b, thick solid lines, thin solid lines, and thin dashed lines indicate boundaries with misorientation angles of >15°, 2–15°, and <2°, respectively. It is clear that the lamellar boundaries are dominated by high-angle boundaries (>15°), while most of the interconnecting boundaries are low-angle ones (<15°). Such an analysis was made for three areas, and in total misorientation angles for more than 300 boundary segments were analyzed. The distribution of these misorientation angles is shown in the histogram, Fig. 1c, covering the entire range from low to high angles. Such a distribution is similar to that determined by TEM methods in other nanostructured metals [1–7]. The average misorientation angle (θ_{av}), the fraction of high-angle boundaries (>15°), and the fraction of boundaries below 2° are listed in Table 1. It is seen that the fraction of high angles is high (~60%) but that of the lowest angles (<2°) is also significant (11%).

The presence of loose dislocations was observed in the volume between the boundaries, which is clearly seen in many of the lamellae in Fig. 2. The dislocation density varies from crystallite to crystallite and the average dislocation density, ρ_0, was determined to be 6.3×10^{13} m^{-2} (Table 1). Such a low-dislocation density is probably due to an enhanced recovery during the ARB processing at a warm temperature (500 °C). Note that this dislocation

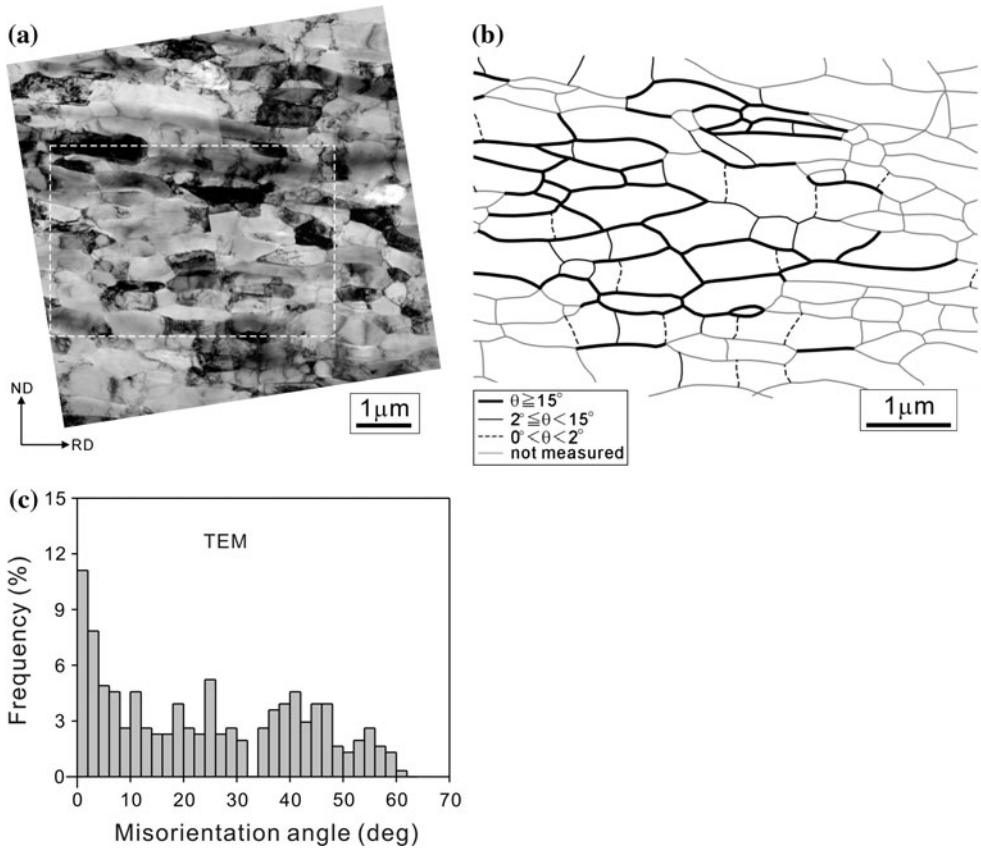

Fig. 1 **a** TEM image showing a typical lamellar structure in the nanostructured IF steel produced by 6 cycles of ARB at 500 °C. **b** A sketch of the boundaries seen in the frame indicated in (**a**), showing the distribution of high-angle and low-angle boundaries in the structure. **c** Distribution of misorientation angles obtained from TEM Kikuchi diffraction

Table 1 Structural parameters of nanostructured IF steel samples after different treatments

Sample state	d_t (nm)	d_l (nm)	θ_{av} (°)	$f(\theta \geq 15°)$ (%)	$f(\theta < 2°)$ (%)	ρ_0 (m^{-2})
As-ARB	210	620	24.2	59.8	11.1	6.3×10^{13}
ARB + 400 °C for 30 min	220	650	–	–	–	4.0×10^{13}

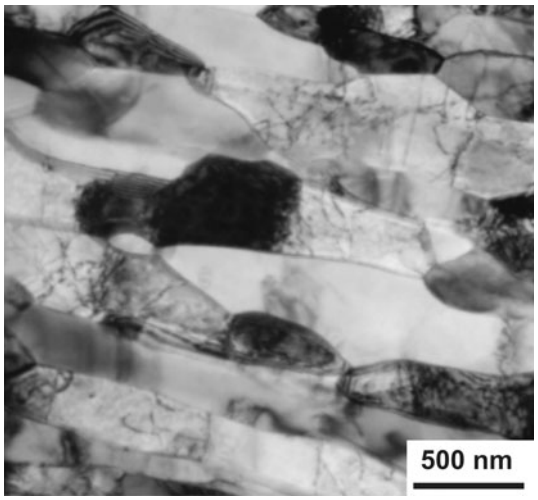

Fig. 2 High-magnification TEM view showing the presence of loose dislocations in the volumes between the boundaries in a 6-cycle ARB IF steel sample

density is even lower than that determined for a nanostructured Al produced by a 6-cycle ARB at room temperature [4].

The stress–strain curve for the ARB sample is shown in Fig. 3, curve 1, which is similar to that reported previously [21] for a nanostructured IF steel sample ARB processed under similar conditions. As compared with the starting material ($\sigma_{0.2} = 142$ MPa and $\sigma_{UTS} = 276$ MPa), significant strengthening by ARB is achieved ($\sigma_{0.2} = 633$ MPa and $\sigma_{UTS} = 895$ MPa). However, the necking starts at a small strain <2%, followed by a quick decrease in the flow stress and fracture, and the total elongation is about 4%.

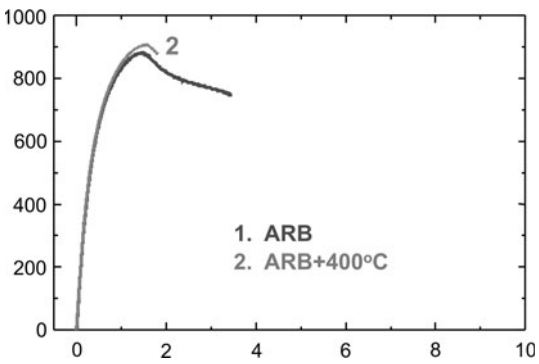

Fig. 3 Engineering stress–strain curves for nanostructured IF steel samples processed by 6-cycle ARB at 500 °C and annealed for 30 min at 400 °C

Samples annealed for 30 min at 400 °C

Figure 4 shows the TEM structure of the sample annealed for 30 min at 400 °C. This annealing treatment led to further recovery of the dislocations, but no significant structural coarsening was observed, see Table 1.

The stress–strain curve of this annealed sample, curve 2 in Fig. 3, is compared with that of the as-ARB processed sample. The yield stress and the UTS increased to 676 and 909 MPa, respectively, but the total elongation decreased to 1.6% after annealing. This annealing-enhanced flow instability is in agreement with previous observations in nanostructured Al processed by ARB [4, 13, 19] or equal channel angular pressing (ECAP) [23, 24].

Effect of cold rolling strain

Figure 5 shows TEM images of the samples annealed followed by cold rolling to 15% (a) and to 50% (b)

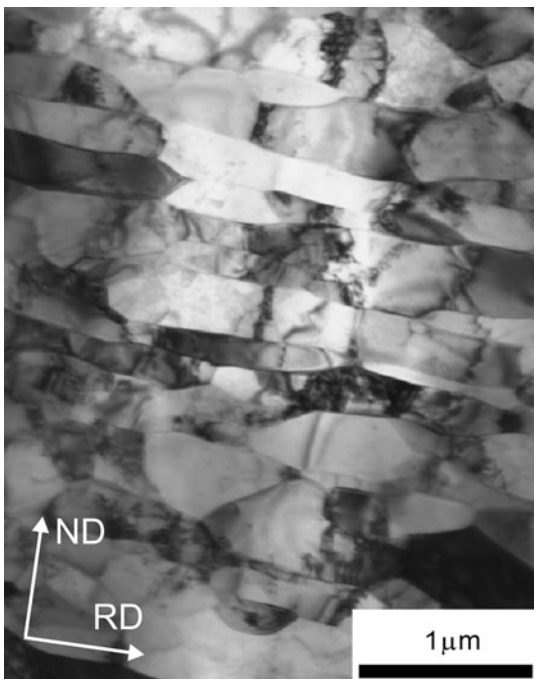

Fig. 4 TEM structure of the same material as Fig. 1a + annealing for 30 min at 400 °C

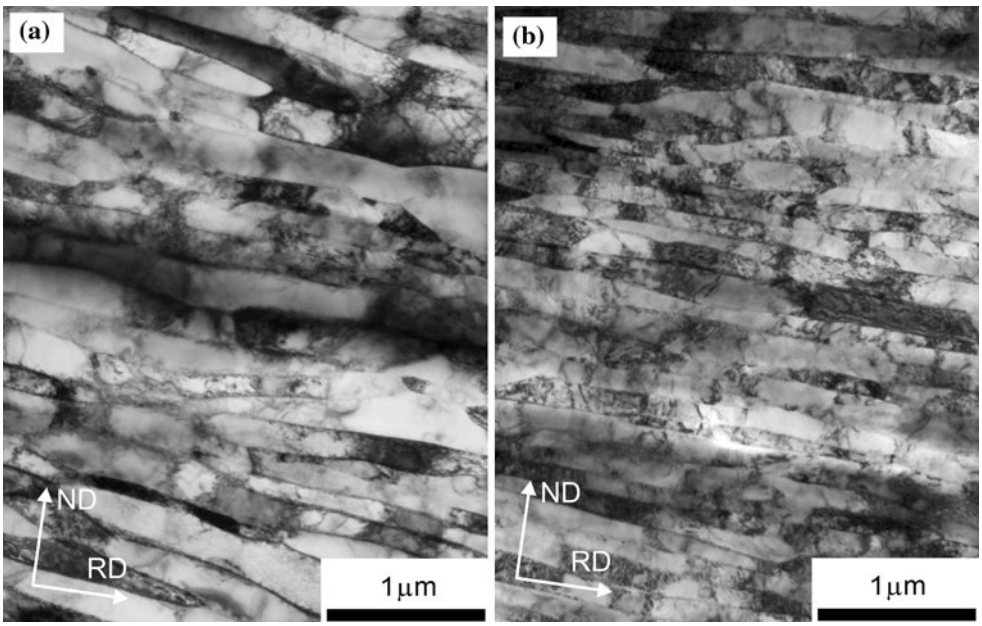

Fig. 5 TEM images showing the deformed structure of samples after different post-process treatments, **a** the same material as Fig. 4 + 15% cold rolling, **b** the same material as Fig. 4 + 50% cold rolling

thickness reductions. Compared with the annealed sample (Fig. 4), several structural changes were found based on morphological observations and TEM quantification of lamellar boundary spacing, interconnecting boundary spacing, and density of the dislocations present in the volume between boundaries. Close observations of the dislocation configurations showed that in the 15% cold-rolled sample the dislocations are mostly present as isolated dislocations and the extent of dislocation tangling is not significant. However, with an increase in the rolling reduction to 50%, dislocation tangles and networks were often observed within the lamellae, indicating a strong interaction between dislocations. Figure 6 shows the changes of the lamellar boundary spacing and the interconnecting boundary spacing. It is seen that the lamellar boundary spacing decreases significantly and almost follows the geometrical reduction in the sample thickness, indicating that applying cold rolling to an annealed ARB sample is an efficient way to achieve further refinement. Moreover, the interconnecting boundary spacing also decreases with an increase in rolling strain from 15 to 50%. This suggests that new interconnecting boundaries are formed during this rolling stage, which is a result of interactions of dislocations introduced in the narrow volumes between the lamellar boundaries. Figure 7 shows the variation of the dislocation density with strain, revealing a significant increase after 50% cold rolling.

Figure 8 shows the stress–strain curves of samples of (i) as-annealed and (ii) as-annealed followed by cold rolling. It is seen that deformation by 5–15% cold rolling induces a

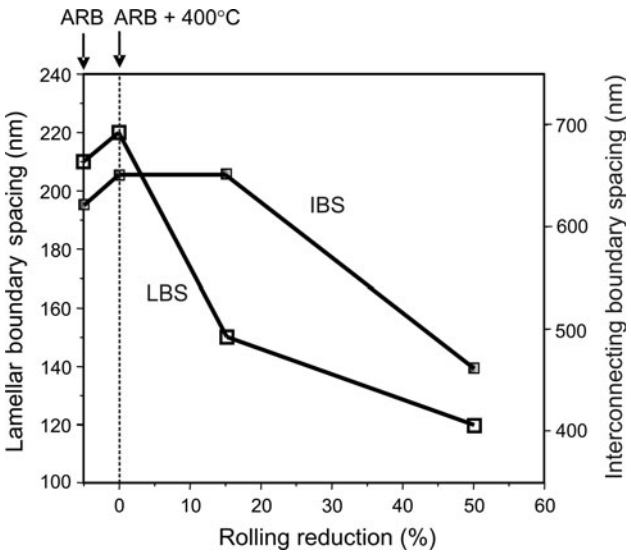

Fig. 6 Lamellar boundary spacing (LBS) and interconnecting boundary spacing (IBS) versus cold rolling reduction. The data for a 6-cycle ARB sample and a 400 °C annealed sample are included for comparison

clear decrease in the strength and a significant enhancement in the elongation (curves 2, 3, and 4) as compared with the annealed sample (curve 1). Remarkably, after 30% cold rolling (curve 5), the yield strength and UTS are comparable with those of the annealed sample (curve 1), but the uniform elongation and the total elongation are significantly larger than those of the annealed sample (curve 1). Further strengthening is observed after 50% cold

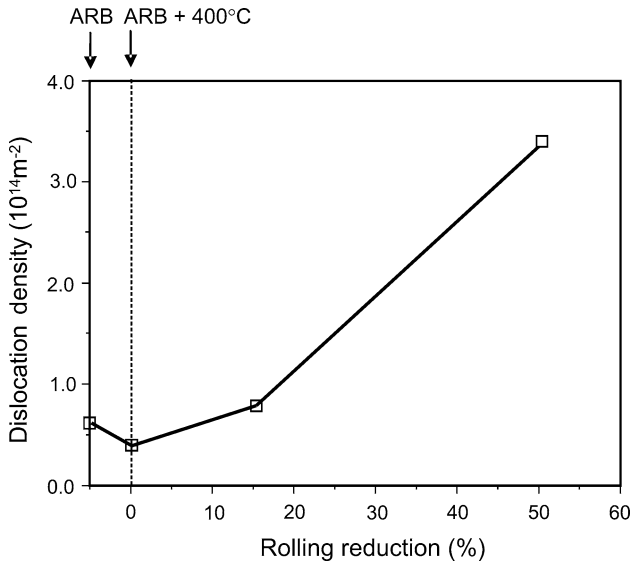

Fig. 7 Variation of dislocation density as a function of cold rolling reduction. The data for the 6-cycle ARB sample and the 400 °C annealed sample are included for comparison

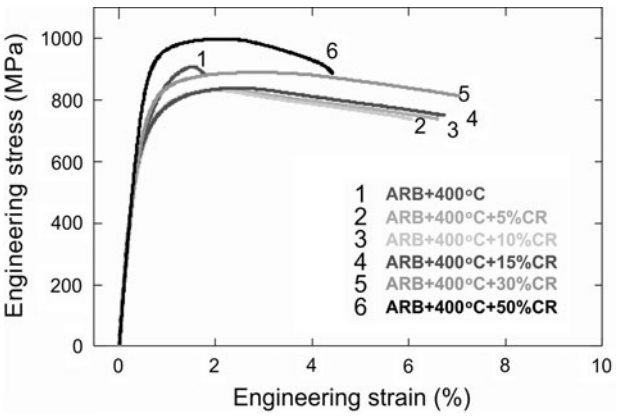

Fig. 8 Engineering stress–strain curves for nanostructured IF steel. *Curve 1*: processed by 6-cycle ARB and annealed at 400 °C for 30 min. *Curve* 2: same material as 1, plus 5% cold rolling. *Curve 3*: same material as 1, plus 10% cold rolling. *Curve 4*: same material as 1, plus 15% cold rolling. *Curve* 5: same material as 1, plus 30% cold rolling. *Curve 6*: same material as 1, plus 50% cold rolling

rolling (curve 6); the sample shows a stress level higher than all the other samples over the entire plastic strain range until fracture occurs. Figure 9 shows the strength (a) and elongation (b) determined from the stress–strain curves as a function of the rolling reduction, which reveals that both the strength and elongation are better in the samples cold-rolled by 30–50% than the samples as-ARB processed and annealed, indicating a simultaneous improvement of strength and ductility.

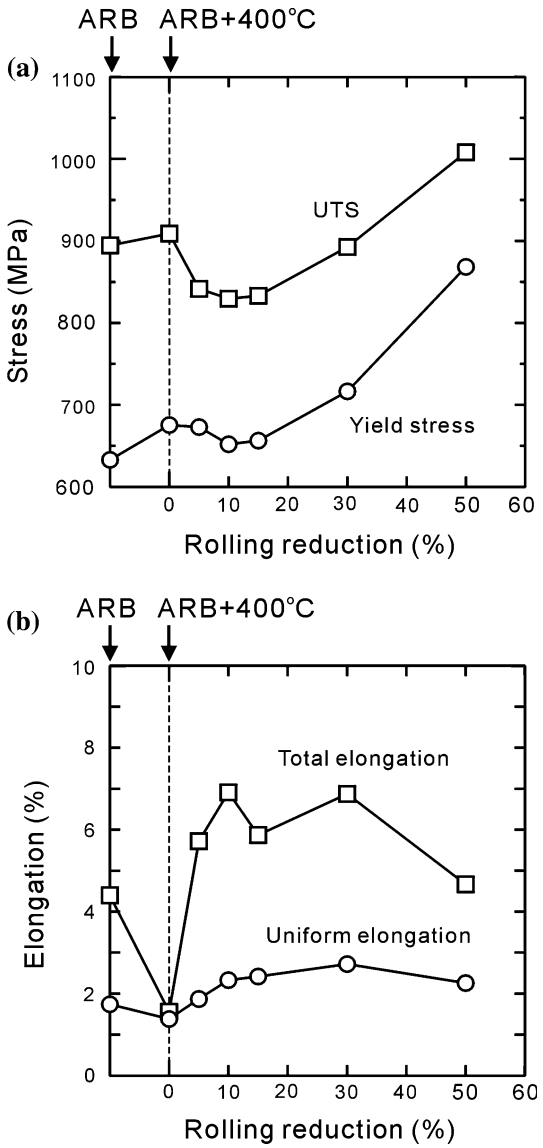

Fig. 9 Effect of cold rolling reduction on the strength (**a**) and elongation (**b**) of nanostructured IF steel

Discussion

Dislocation source limited strengthening

The present study demonstrated that annealing-induced hardening occurs in nanostructured IF steel produced by ARB, Fig. 3, in good agreement with the results of nanostructured aluminum produced by ARB [4, 19] or ECAP [23, 24]. The TEM observations indicate that the dominating microstructural change during the low-temperature annealing treatment is a decrease in the dislocation density (Fig. 4 and Table 1), whereas the change in boundary spacing is insignificant. It is, therefore, suggested that the decrease in the dislocation density is the main cause for the observed hardening.

As shown in Fig. 1a, b, the as-ARB sample is characterized by closely spaced high-angle boundaries that may act as dislocation sinks, so that a subsequent low-temperature anneal may easily reduce the density of individual dislocations between the boundaries [4]. The low-temperature annealed sample may, therefore, contain few mobile dislocations. A higher stress is, therefore, required to activate alternative dislocation sources to deform the sample when tensile tested, which can rationalize the observed behavior. This strengthening mechanism has been recognized in nanostructured Al [4], and referred to as "dislocation source limited strengthening" [19].

One may argue that the annealing-induced hardening is due to an impurity effect, such as boundary segregation or precipitation. An impurity effect cannot be ruled out completely and may operate to some extent in the present material. However, softening observed after a light rolling deformation of the annealed sample points strongly to a dislocation-related phenomenon. This is underpinned by the TEM observations showing that a large amount of dislocations have been re-introduced into the sample by 15% rolling (Fig. 5a). Therefore, yielding may occur at a lower stress, consistent with the hypothesis of dislocation source limited strengthening, where the lack of mobile dislocations and dislocation sources leads to an increase in the tensile strength.

The dislocation source limited strengthening was analyzed in detail in high-purity aluminum (99.99%) ARB processed and annealed [19], and it appears that this mechanism operates over the grain size range where enhanced localized shear deformation (Lüders banding) occurs. The grain size range for the ARB 99.99% pure Al covers from a few hundred nanometers to about 10 μm, while a relatively smaller upper limit of grain size may occur in ARB 99% pure Al as the localized shearing disappears when the grain size is above about 5 μm [13]. Recognizing the grain size range for the dislocation source limited strengthening mechanism to occur will provide guidance for the exploration of stabilizing the mechanical flow by introducing mobile dislocations in the structure [25].

Softening versus hardening by post-process deformation

The present results show that the effect of post-process deformation on the yield strength of nanostructured IF steel is not a monotonic function of the rolling reduction. As shown in Fig. 9, the yield strength decreases with strain in the low-strain range, followed by a gradual increase with further straining. This observation is very similar to that observed in nanostructured Al, which experienced similar post-process annealing and deformation treatments [26]. These results suggest that a deformation-induced decrease in the yield strength (softening) in the nanostructured metals occurs only when the strain is lower than a certain value, and a deformation-induced increase in the yield strength (hardening) takes place again when the strain is above this value. The critical strain at which the transition from deformation-induced softening to hardening takes place may depend on the material and structural parameters such as the boundary spacing, the high-angle boundary fraction and the initial dislocation density. For the present nanostructured IF steel samples, the transition strain is about 30% (see Fig. 9), which is similar to that identified in nanostructured 99.2% pure Al [26]. This transition strain corresponds to a dislocation density of about 2×10^{14} m^{-2} (Fig. 7), which is higher than the dislocation density in the as-ARB sample. Therefore, a light deformation of the as-ARB sample will cause a decrease in the yield strength, which was observed previously [20]. The transition strain may depend on the dislocation density in the initial microstructure and on how efficient the mobile dislocations introduced during the post-process deformation are stored in the grains. It is expected that when the density of dislocation sinks is increased, e.g., by increasing the fraction of high-angle boundaries per volume, the transition strain will be increased. If the initial dislocation density is too high (higher than that corresponding to the transition strain), the deformation-induced decrease in the yield strength may not occur, instead strain hardening will take place.

This dependence of the occurrence of a deformation-induced decrease or increase in the yield strength (softening or hardening) on the post-process strain must relate to an internal change in the dislocation structure. The introduction of mobile dislocations and dislocation sources by a light cold rolling has been proposed to be the cause for the deformation-induced softening in nanostructured materials [4, 27]. This explains the observation of a rather significant decrease in the yield stress in the 5–15% deformed samples as loose dislocations are introduced in these samples (e.g., Fig. 5a). However, when a higher density of dislocations is introduced into the sample, they interact with each other forming strong tangles and network (Fig. 5b). As a result, both the density of the dislocations that is free to move when a stress is applied and the free length of dislocation segments that can act as dislocation sources decrease. Therefore, the softening effect by mobile dislocations and easy dislocation sources is reduced and a large portion of the dislocations present in such a structure will contribute to a dislocation forest hardening, leading to a net increase in strength and a decrease in elongation.

Another remarkable effect of the post-process cold rolling is seen in the increase of both the uniform and post-necking elongation (Figs. 8 and 9b). The engineering

stress–strain curves of post-process deformed samples (curves 2–6 in Fig. 8) show a fairly gradual decrease of the stress with necking strain. An examination of the change in thickness and width of deformed samples confirmed a smooth necking. Figure 9b shows that the ductility enhancement is dominated by the increase in post-necking elongation. These observations indicate that the flow stress of the post-process deformed samples possesses an enhanced sensitivity to the strain rate, which helped stabilize the tensile deformation. Quantitative evaluation of the strain rate sensitivity for both the annealed and post-process cold-rolled samples are undertaken, which will be reported in a forthcoming paper with an aim to further analyze the effects of strain hardening and strain rate hardening on the mechanical behavior of annealed and post-process deformed samples.

Property optimization by post-processing deformation

Our previous study on nanostructured fcc aluminum [26] has demonstrated that an appropriate post-process deformation can improve both strength and ductility. The present results in a bcc IF steel show a similar effect of a post-process deformation. As seen in Fig. 9, both strength and ductility in the 30 and 50% deformed samples are better than those of the as-ARB sample and the annealed sample. It is interesting to note that for both the nanostructured Al samples investigated in the previous study [26] and the nanostructured IF steel investigated in the present study, the structural parameters required to achieve a simultaneous improvement of strength and ductility are similar, namely a high fraction of high-angle boundaries (60–70%), an average lamellar spacing of 100–200 nm, and a dislocation density of $1–3 \times 10^{14}$ m^{-2}. Similar structural parameters were reported [12] for toughening an ultrafine grained Cu sample. Further identification and verification of such structural conditions are being undertaken by a new experimental design, with an expectation to provide a general guidance for optimizing strength and ductility by tailoring structural parameters.

Conclusions

In order to understand the strengthening mechanisms and to identify the structural conditions for optimization of mechanical properties of nanostructured metals, a series of nanostructured IF steel samples have been prepared by ARB at 500 °C followed by post-process treatments by annealing at 400 °C and cold rolling up to 50% thickness reductions, and characterized by TEM and tensile testing. Based on the present results and previous results obtained in nanostructured Al produced by ARB, the following conclusions can be drawn.

1. The nanostructured IF steel processed by a warm ARB process contained a high fraction of high-angle boundaries and a low density of dislocations between the boundaries, which was further decreased after a recovery anneal at 400 °C. A dislocation source limited strengthening mechanism was found to operate in both cases, enhancing the localized shear deformation followed by low-tensile elongation.
2. By applying cold rolling to an annealed IF steel sample produced by ARB both the flow stress and the elongation can be significantly changed and optimal properties have been obtained (Fig. 9) for samples with a structural scale of 100–200 nm, a fraction of high-angle boundaries of about 60–70%, and a dislocation density of $1–3 \times 10^{14}$ m^{-2}.
3. The observed effects of annealing and deformation on ARB processed IF steel and aluminum suggest that important parameters when tailoring the structure and mechanical properties are a small spacing between deformation-induced high-angle boundaries, which can act as sinks for mobile dislocations and a relatively low-dislocation density to reduce strain hardening when dislocations are intentionally introduced by deformation.

Acknowledgements We acknowledge the Danish National Research Foundation for supporting the Danish-Chinese Center for Nanometals, within which this work was performed. We also thank Prof. B. Ralph for his careful reading of the manuscript and suggestions for language corrections.

References

1. Hughes DA, Hansen N (2000) Acta Mater 48:2985–3004
2. Liu Q, Huang X, Lloyd DJ, Hansen N (2002) Acta Mater 53:3789
3. Mishin OV, Juul Jensen D, Hansen N (2003) Mater Sci Eng A 342:320
4. Huang X, Hansen N, Tsuji N (2006) Science 312:249
5. Kamikawa N, Tsuji N, Huang N, Hansen N (2006) Acta Mater 54:3055
6. Cabibbo M, Blum W, Evangelista E, Kassner ME, Meyers MA (2007) Metall Mater Trans A 39:181
7. Zhang HW, Huang X, Hansen N (2008) Acta Mater 56:5451
8. Wu XL, Ma E (2006) Appl Phys Lett 88:231911
9. Zhao YH, Zhu YT, Liao XZ, Horita Z, Langdon TG (2006) Appl Phys Lett 89:121906
10. Zhao YH, Bingert JF, Liao XZ, Cui BZ, Sergueeva AV, Mukherjee AK, Valiev RZ, Langdon TG, Zhu YT (2006) Adv Mater 18:2949
11. Huang X (2007) J Mater Sci 42:1577. doi:10.1007/s10853-006-0988-5
12. Zhao YH, Bingert JF, Zhu YT, Liao XZ, Valiev RZ, Horita Z, Langdon TG, Zhou YZ, Lavernia EJ (2008) Appl Phys Lett 92:081903
13. Tsuji N, Ito Y, Saito Y, Minamino Y (2002) Scr Mater 47:893

14. Zhu YT, Huang JY, Ungar T, Wang YM, Ma E, Valiev RZ (2003) J Mater Res 18:1908
15. Meyers MA, Mishra A, Benson DJ (2006) Prog Mater Sci 51:427
16. Koch C, Ovid'ko I, Seal S, Veprek S (2007) Structural nanocrystalline materials—fundamentals and applications. Cambridge University Press, Cambridge
17. Hansen N (2004) Scr Mater 51:801
18. Hansen N (2005) Adv Eng Mater 7:815
19. Kamikawa N, Huang X, Tsuji N, Hansen N (2009) Acta Mater 57:4198
20. Huang X, Kamikawa N, Hansen N (2008) Mater Sci Eng A 493:184
21. Winther G, Huang X, Godfrey A, Hansen N (2004) Acta Mater 51:4437
22. Liu Q (1995) Ultramicroscopy 60:81
23. Bowen JR, Prangnell PB, Juul Jensen D, Hansen N (2004) Mater Sci Eng A 387389:235
24. Yu CY, Kao PW, Chang CP (2005) Acta Mater 53:4019
25. Huang X (2009) Scr Mater 50:1078
26. Huang X, Kamikawa N, Hansen N (2008) J Mater Sci 43:7397. doi:10.1007/s10853-008-2873-x
27. Huang X, Kamikawa N, Hansen N (2008) Mater Sci Eng 483–484:102